THE JOURNAL OF PHYSICAL CHEMISTRY Letters

pubs.acs.org/JPCL

Obtention of Metallic Nanowires by Protein Biotemplating and Their Catalytic Application

Josué Juárez, Adriana Cambón, Sonia Goy-López, Antonio Topete, Pablo Taboada,* and Víctor Mosquera

Grupo de Física de Coloides y Polímeros, Departamento de Física de la Materia Condensada, Facultad de Física, Universidad de Santiago de Compostela, E-15782 Santiago de Compostela, Spain

ABSTRACT Gold nanowires were obtained by a seeded growth process using protein lysozyme fibrils as biotemplates. The degree of metal coverage until full biotemplate coverage onto the fibril was controlled by the gold salt concentration and the number of sequential additions of metal growth solutions. The hybrid fibrils might have a potential use as catalysts since they display enhanced catalytic activity in the reduction of *p*-nitrophenol to *p*-aminophenol by $NaBH_4$.

SECTION Nanoparticles and Nanostructures

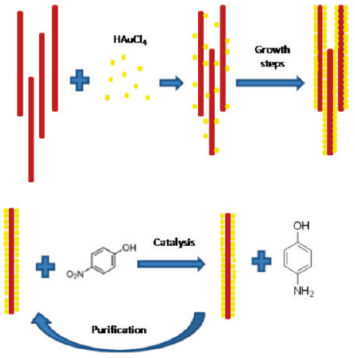

Metal nanoparticles have received considerable attention in past decade because of their particular optical, electronic, magnetic, and catalytic properties and their important applications in many fields such as nanosensors,[1−4] catalysis,[5−8] biomedicine,[9−11] biological labeling,[12−14] and surface-enhanced Raman scattering (SERS).[15−18] To optimize and extend the application of metal NPs, methods must be developed to control the assembly and organization of these nanomaterials. Assemblies of NPs provide optical and electronic properties that are distinct compared to individual particles or disorganized macroscale agglomeration. In this regard, Nature offers us the possibility to take advantage of the well-defined structures and special properties of biomolecules and their supramolecular structures to organize nanoparticles into predefined, topologically intricate nanostructures or to synthesize miscellaneous materials in order to control the properties of nanoparticle assemblies for potential applications in electronic, optical, and chemical devices.[19−23] In particular, functionalizing one-dimensional (1D) supporting biomaterials with metal NPs that combine the properties of two functional nanomaterials, such as high conductivity surface area or precise chemical functionality of the biotemplate and the unique plasmonic or catalytic properties of metal NPs, to achieve a wider range of applications will therefore play an important role in the development of nanoscience and nanotechnology. As a result, considerable efforts have been directed toward the use of 1D biotemplates such as DNA,[24−27] viruses,[28−31] peptides,[32−34] proteins,[35−38] or fungus[39] to construct corresponding multifunctional hybrid 1D nanostructures such as nanowires,[40−43] nanotubes,[44−46] or nanodumbbells.[47]

The spontaneous fibrillation mechanism which different proteins undergo under suitable conditions results in the formation of amyloid-like fibrils,[37,48,49] which should be valid as alternative templating agents for the construction of 1D hybrid materials. In particular, lysozyme (Lys) is a protein which is known to fibrillate under different solution conditions to form protein fibrils with diameters ranging from 10 to 50 nm and lengths up to several micrometers (see Figure 1a).[50−52] The dimensions of the fibrils can be tuned by varying the solution conditions and the incubation time. They are also thermally stable at high temperatures and different pHs, and they contain multiple potential ion-binding sites within their amino acid sequences, which enables their use in metallization reactions under relatively harsh conditions. Thus, we exploit all of these features to generate 1D nanoparticle assemblies and nanowires by in situ nanoparticle formation and seeding growth on the fibril surface and to analyze their potential applicability as biocatalysts.

Although biotemplating of 1D metallic nanoparticle assemblies and nanowires by peptides and protein fibrils has been previously reported[35,37,38,40,43] and their electric and magnetic properties have been evaluated,[35,53] less attention has been paid to the obtention of 1D protein-fibril-templated metallic nanostructures with a controlled degree of metallization and their potential application as a catalyst. Here, we present a seeded-mediated method for the controlled coverage by Au NPs on the surface of the fibrils formed by the protein Lys in order to find the optimal conditions for the use of the present biohybrid systems as a catalyst. We test their catalytic capability using the model reduction reaction of *p*-nitrophenol by $NaBH_4$.

Lys fibrils were prepared as previously described (see Experimental Section). Au-nanoparticle-coated protein fibrils were obtained by the addition of preformed citrate-stabilized Au seeds to an aqueous solution containing self-assembled fibrils at pH 2.0. Provided that the isoelectric point of Lys is around 11,[54] it is expected that negatively charged gold seed

Received Date: July 26, 2010
Accepted Date: August 23, 2010
Published on Web Date: August 31, 2010

DOI: 10.1021/jz101029f | *J. Phys. Chem. Lett.* **2010**, *1*, 2680–2687

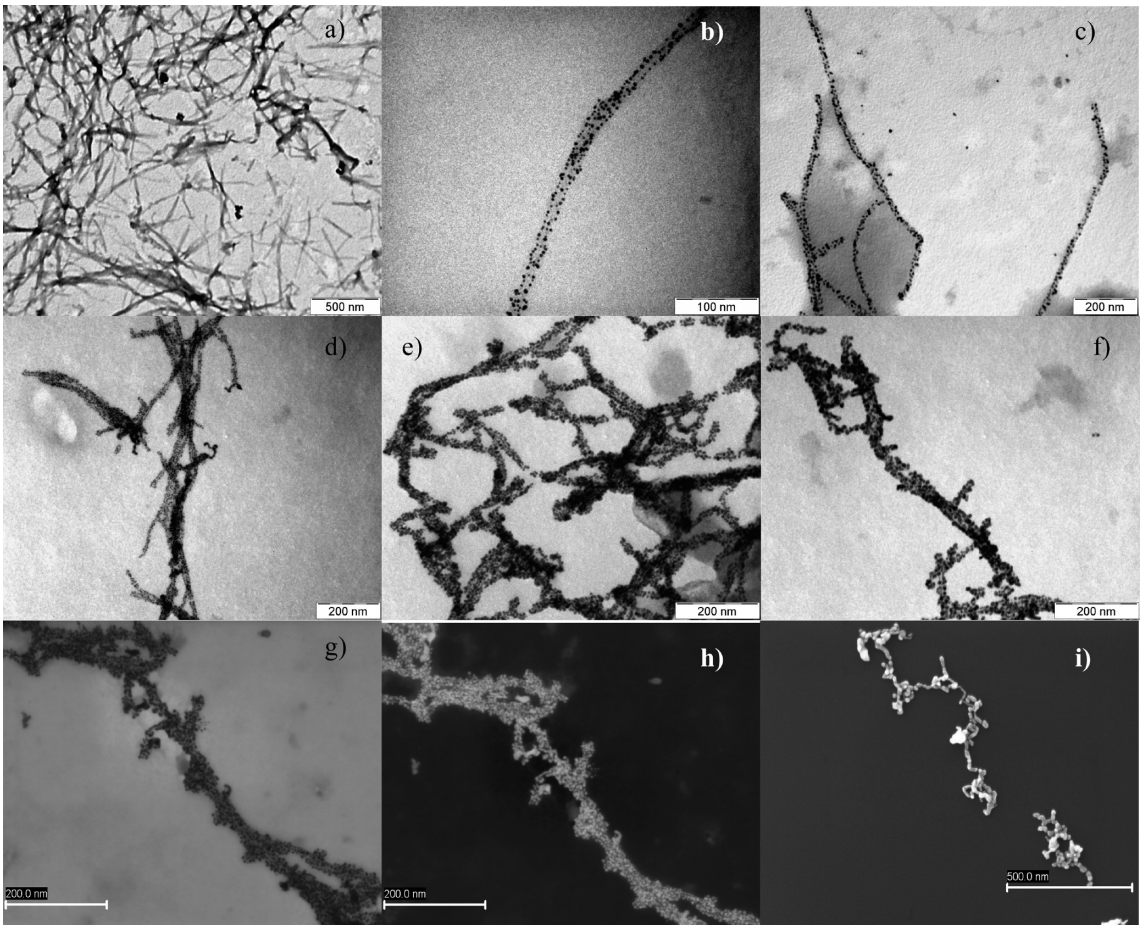

Figure 1. TEM images of (a) bare Lys fibrils and Au−fibril biohybrids obtained after (b) zero, (c) one, (d) two, (e) three, and (f) four sequential additions of the Au growth solution; (g) bright field and (h) dark field TEM images of fully covered fibrils; (i) SEM image of a Au−metallic biohybrid nanowire. Scale bars are (a,i) 500, (b) 100, and (c−h) 200 nm.

Table 1. Au Content of the Obtained Nanohybrids

sample ([Au]/[protein] MR)	Au concentration (10^{-5} M)
biohybrid 1(50)	3.4
biohybrid 2 (100)	3.9
biohybrid 3 (125)	4.6
biohybrid 4 (150)	5.3
biohybrid 5 (200)	6.0

ions would interact electrostatically with electrically charged amine groups located at the fibril surfaces after incubation. Subsequently, different sequential additions of a solution containing $HAuCl_4$ and ascorbic acid were performed in order to achieve a full coverage of the hybrid composites. Different initial [Au seeds]/[protein] molar ratios (MR) were tested in order to find an initial suitable MR to ensure full coverage after a few additions and to avoid both precipitation of the nanohybrid and the generation of free gold NPs. An initial [Au seed]/[protein] MR = 50 was found to be the optimal one and was further used during the sequential additions of Au ions to achieve the formation of the metallic nanowires (see Table 1).

The morphologies of the resulting products were investigated by transmission electron microscopy (TEM) and scanning transmission microscopy (SEM). Figure 1a shows a typical TEM image of the as-prepared Lys fibrils, with lengths ranging from 0.4 to 8 μm and widths of 12−20 nm. The metallic coverage of the nanofibrils could be easily controlled by changing the number of sequential additions of gold growth solution into the fibril solution over already preformed Au nanocrystals. Figure 1b−e shows the progressive coverage of the nanofibrils after increasing the number of sequential additions, with the formation of more metallic nanoparticles onto the fibril surface. TEM revealed that metallic nanoparticles on the fibril surfaces possess a size ranging from 3.7 to 8.0 ± 2.0 nm, depending on the number of sequential additions of the gold growth solution. The continuous coverage is a result of the growth of pre-existing NPs and generation of new ones on the fibril surface and subsequent fusion of adjacent as-synthesized NPs. The fully covered fibrils display a relatively rougher surface than pristine and partially covered fibrils, as can be observed from the TEM image obtained in the backscattering mode and the SEM picture obtained without the need for metallic contrast (see Figure 1h,i). Also, the size of the metallic NPs clearly increases, and the size population can also broadened (see Figure S1, Supporting Information). In addition,

DOI: 10.1021/jz101029f | J. Phys. Chem. Lett. 2010, 1, 2680–2687

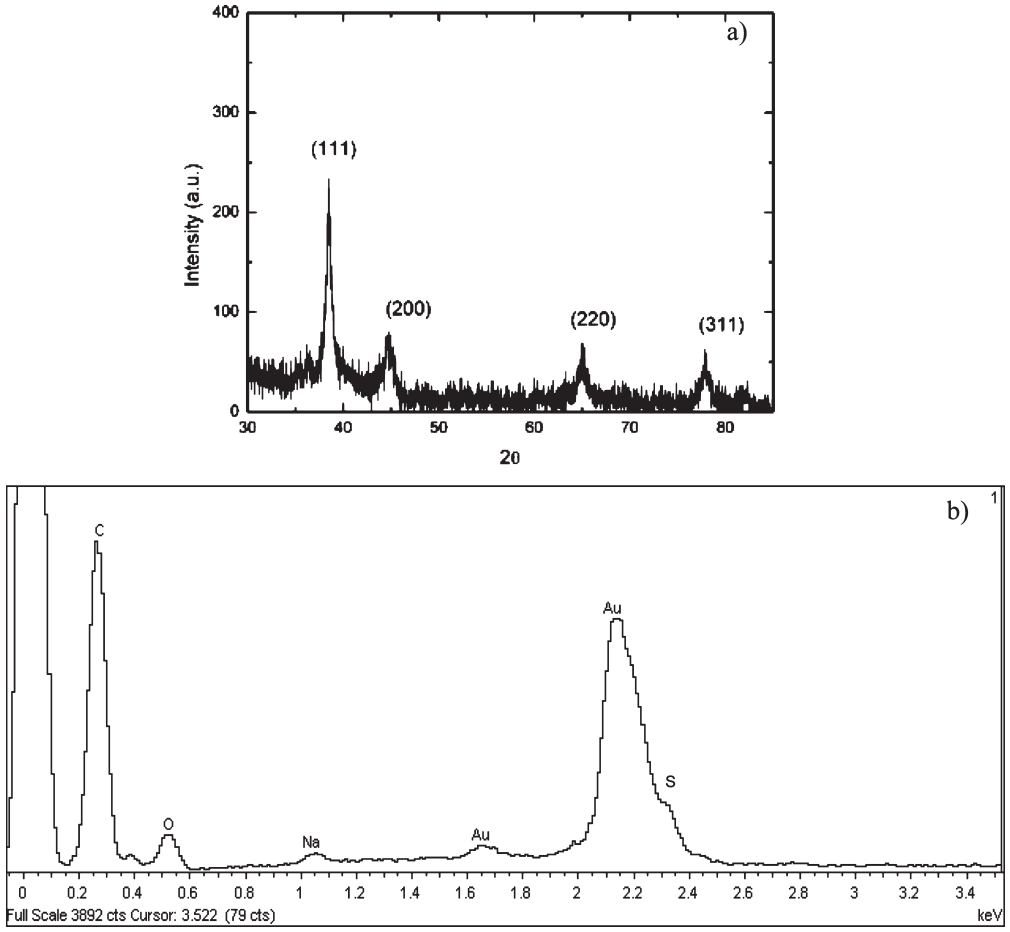

Figure 2. (a) XRD pattern of spherical Au NPs on the surface of protein fibrils; (b) EDX pattern of a gold hybrid fibril.

under conditions of excessive addition of Au ions in solution, an increasing presence of fibril networks is observed as a consequence of fibril bundling, which leads to precipitation of the nanowires after several days (see Figure S2, Supporting Information).

The formation of hybrid fibrils was further characterized by energy dispersive X-ray (EDX) spectroscopy and X-ray diffraction (XRD). XRD patterns of the resulting hybrid fibrils display the classical peaks corresponding to metallic spherical gold NPs. The crystallite sizes calculated according to the modified Scherrer relation[55] for the hybrid fibrils range from 5 to 8 nm depending on the number of additions of Au growth solution. The EDX spectrum (Figure 2b) of protein-fibril-supported Au NPs shows the peaks corresponding to C, O, S, and Au, confirming the existence of Au NPs on the surface of the Lys fibrils. The S peak is characteristic of protein samples.[56]

To study the performance of the Au NP hybrid fibrils as catalysts, we have chosen the borohydride reduction of *p*-nitrophenol as a model reaction. It is well documented that this reaction can be catalyzed by noble metal nanoparticles, and the color changes involved in the reduction also provide a simple way based on spectroscopic measurements for monitoring the reaction kinetics.[57,58] Under a neutral or acidic condition, *p*-nitrophenol solution exhibits a strong absorption peak at 317 nm. Upon the addition of $NaBH_4$, the alkalinity of the solution increases, and *p*-nitrophenolate ions would become the dominating species, together with a spectral shift to 400 nm for the absorption peak.[59,60] This peak remains unaltered with time, suggesting that the reduction did not take place in the absence of a catalyst, as reported elsewhere.[61,62] However, the addition of a small amount of the Au-based catalyst (i.e., metal hybrid fibrils with a Au concentration ranging from 0.002 to 0.02 mM) to the above reaction mixture causes fading and ultimate bleaching of the yellow color of the reaction mixture quickly. Time-dependent absorption spectra of this reaction mixture show the disappearance of the peak at 400 nm that is accompanied by a gradual development of a new peak at 300 nm corresponding to the formation of *p*-aminophenol (Figure 3a). The UV spectra also exhibit an isosbestic point between two absorption bands, indicating that only two principal species, *p*-nitrophenol and *p*-aminophenol, influence the reaction kinetics. Similar spectral changes were also observed with other hybrid fibrils with different Au NP concentrations. These results indicate that the hybrid fibrils can successfully catalyze the reduction reaction. Several research groups have also reported similar kinds of spectral changes of *p*-nitrophenol during its catalytic reduction in the presence of both supported and unsupported spherical metallic nanoparticles.[63−65] In this reduction process, as the concentration of $NaBH_4$ in the reaction mixture far

DOI: 10.1021/jz101029f | J. Phys. Chem. Lett. 2010, 1, 2680–2687

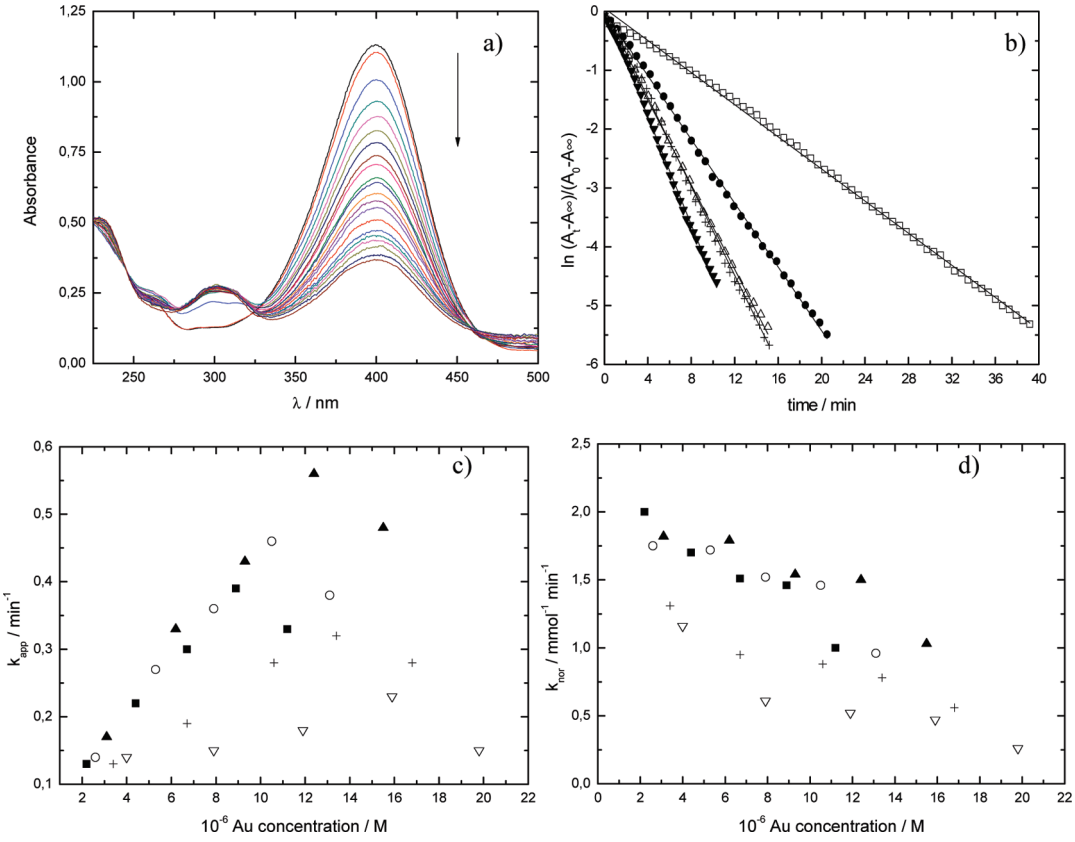

Figure 3. (a) Time evolution of UV−vis spectra and (b) variation of absorbance with time upon conversion of *p*-nitrophenol to *p*-aminophenol in the presence of biohybrid 2 with Au concentrations of (□) 0.26, (●) 0.53, (△) 0.79, (▼) 1.05, and (+) 1.31 × 10^{-5} M. The arrow in (a) denotes the decreasing presence of *p*-nitrophenol in the mixture as the reduction reaction proceeds. Variation of (c) k_{app} and (d) k_{nor} with Au concentration present in the reduction reaction: (■) biohybrid 1, (○) biohybrid 2, (▲) biohybrid 3,; (+) biohybrid 4, and (▽) biohybrid 5.

exceeds the concentration of *p*-nitrophenol, the reaction rate is assumed to follow first-order kinetics. Keeping this in mind, we decided to measure the concentrations of *p*-nitrophenolate ions and thus to monitor the progress or kinetics of the reaction by recording the absorbance at 400 nm because the latter peak was much stronger than that at 315 nm. We calculated the values of the apparent rate constants (k_{app}) of the catalytic reaction in the presence of different concentrations of the hybrid fibrils possessing different degrees of Au coverage from the change of absorbance with time (Figures 3b and S3, Supporting Information). These plots are straight lines, indicating that the reduction reaction effectively follows first-order kinetics. The k_{app} values of the hybrid fibrils rise linearly with an increase of their concentration (and, thus, also with increases in Au concentration) in the reaction medium until reaching a maximum to decrease further (see Figure 3c). In addition, values of k_{app} for *p*-nitrophenol reduction using hybrid fibrils were ∼1.5−4 times larger than those reported for glucose-reduced Au nanoparticle networks,[64] poly(amidoamine) (PAMAM)-dendrimer-supported spherical nanoparticles,[59] solid 1D Au nanobelts[66] and nanorods,[67] polymer-micelle-supported Au NPs,[68,69] multicomponent microgels,[70] and 1D assemblies of Au NPs,[71] and they were of similar order as those obtained for porous 1D nanobelts[66] or Au yolk-shell NPs.[72] Nevertheless, we have to note that we used very small amounts of gold catalysts in our experiments.

Thus, to get a clearer picture of the efficacy of the composite material as a catalyst and also to compare the catalytic activity between hybrid fibrils with different degrees of coverage, the catalytic activities are also presented in terms of a normalized rate constant (k_{nor}) obtained by normalization of k_{app} to the total amount (mmol) of catalyst (gold) used in the reaction. Figure 3d shows that the values of k_{nor} for *p*-nitrophenol reduction in the presence of the different types of hybrid fibrils prepared at different [Au]/[protein] MR values are also different. In particular, k_{nor} remains relatively constant from hybrid 1 to 3, that is, as the coverage of the fibrils increases, while for hybrids 4 and 5, k_{nor} progressively reduces. This behavior might be a consequence of (i) changes in nanoparticle sizes on the fibril surfaces and (ii) a decrease in the available metal surface area for the catalytic reaction to take place as the fibril coverage is almost complete. In this regard, it is well-known that the catalytic activity increases as the size of Au NPs decreases because of the increase of effective surface area. In our case, although the crystallite size increases as the concentration of the growth solution increases, we have noted a larger increase in nanoparticle mean size accompanied with an important polydispersity for nanohybrids 4 and 5, as previously

DOI: 10.1021/jz101029f | J. Phys. Chem. Lett. 2010, 1, 2680–2687

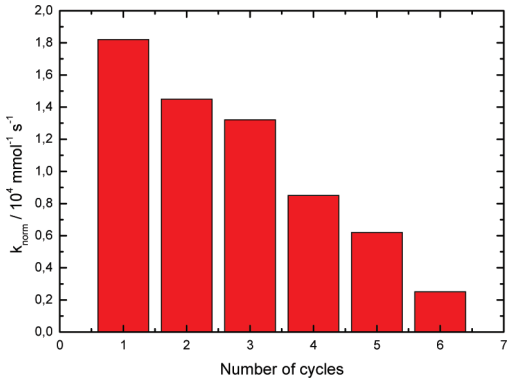

Figure 4. Normalized rate constant (k_{nor}) (with respect to the initial amount of catalyst used) in different cycles of catalytic reduction of *p*-nitrophenol.

mentioned. In addition, for biohybrid 5 fibrils are almost fully covered, which also reduces the accessible metal surface area for reduction to take place. This would explain the decreasing values for such systems. In contrast, hybrids 1, 2, and 3 involve the progressive coverage of the fibrils without a significant increase in crystallite size, which involves an increase in the available metal surface area and, thus, of k_{app}. Interestingly, the k_{nor} values for hybrid fibrils are also 5000 times larger than those obtained for citrate-stabilized gold nanoparticles.[31] In addition, k_{nor} values for the present biohybrids are 2 orders of magnitude larger than those obtained, for example, in the presence of polygonal Au nanostructures,[73] Au−PEDOT/PSS$^-$ composites,[74] or poly(propylene imine) (PPI)-dendrimer-supported spherical nanoparticles.[59] The 1D structure of the protein support can affect more efficiently the adsorption/diffusion of *p*-nitrophenol toward the surface of the gold nanoparticle catalyst, thereby increasing the catalytic activity.[63] Also, the predominance of {111} crystal planes in the nanoparticle structure might also favor the catalytic efficiency.[75]

On the other hand, it is known that reusability is the main advantage of using a heterogeneous catalyst rather than a homogeneous catalyst for industrial applications. To check the reusability of these nanohybrids as catalysts, we have recovered the solid catalyst (e.g., biohybrid 3) from the reaction mixture after completion of the first cycle of nitrophenol reduction by centrifugation. The recovered nanohybrids were stable as confirmed by TEM (Figure S4, Supporting Information). These recovered hybrid nanofibrils were then used as the catalyst in a consecutive run of $NaBH_4$ reduction of nitrophenol, and the k_{app} and k_{nor} of each cycle were calculated as previously. Figure 4 clearly indicates that the activity of the hybrid nanofibrils slightly decreases as the number of reduction cycles increases. However, it is necessary to mention that during the recycling process, a weight loss of ~10% after each reduction cycle occurred. This involved an effective loss of metallic material, which might explain the decrease in catalytic activity compared to that of the pristine hybrid nanofibrils. Also, some increase in fibril bundling due to successive centrifugation steps might also result in a negative influence in the catalytic efficiency of the biohybrid.

In summary, we report a method to obtain metallic Au nanowires by using Lys protein fibrils as bioscaffolds to generate a complete gold coating layer on the biotemplate surface by the attachment of gold seeds and further growth of the coating layer by sequential addition of a gold salt growth solution (seeded-mediated mechanism). To obtain full coverage of the protein fibrils, a suitable initial [Au]/[protein] MR must be selected, and a suitable number of sequential additions of Au ions must be performed. If these requirements are not fulfilled, partial coverage and/or protein bundling and further fibril precipitation are observed. The hybrid metallic fibrils have been proved to be useful as catalytic substrates, provided their superior catalytical activity when incorporated in the reduction reaction of *p*-nitrophenol to *p*-aminophenol by $NaBH_4$. The reaction rates obtained were 1.5−4 times larger than those reported for glucose-reduced Au nanoparticle networks, (PAMAM)-dendrimer-supported spherical nanoparticles, solid 1D Au nanobelts and nanorods, polymer-micelle-supported Au NPs, multicomponent microgels, or 1D assemblies of Au NPs. Also, the hybrid fibrils maintained their catalytical activity when recovered after several cycles of *p*-nitrophenol reduction.

EXPERIMENTAL SECTION

Materials. Lys and $HAuCl_4$ were obtained from Sigma Chemical Co. The protein was used after further purification by liquid chromatography using a Superdex 75 column equilibrated with 0.01 M phosphate. All other chemicals were of the highest purity available. Experiments were carried out using doubly distilled, deionized, and degassed water.

Preparation of Lys Fibril Solutions. Protein fibril solutions were prepared according to previously well-established protocols.[50−52] Briefly, Lys fibrils were obtained by forming a 2 mg/mL stock solution in glycine buffer of pH 2.0 (ionic strengths: 136.7 mM NaCl, 2.68 mM NaCl). Protein stock solution was dialyzed extensively against proper buffer. Protein concentrations were determined spectrophotometrically using a molar absorption coefficient of 37609 at 280 nm.[76] Before incubation, the solutions were filtered through a 0.2 μm filter into sterile test tubes. Samples were incubated at 55 °C in a refluxed reactor for 3 days.

Characterization of the Fibrils. Protein suspensions were applied to carbon-coated copper grids, blotted, washed, negatively stained with 2% (w/v) of phosphotungstic acid, air-dried, and then examined with a Phillips CM-12 transmission electron microscope operating at an accelerating voltage of 120 kV. Samples were diluted between 20- and 200-fold where needed prior to deposition on the grids.

Au Seed Solution. A volume of 0.06 mL of a $HAuCl_4$ solution (0.025 M) was set in a glass vial. Immediately, 3 mL of sodium citrate (1 mM) and 26 mL of Milli Q water were added, and the mixture was stirred for 15 min. After, 1 mL of a $NaBH_4$ solution (1 M) was added under agitation, and the reduction reaction was conducted. Excess reagents were eliminated by extensive dialysis.

Metallic Nanowire Synthesis. In a typical synthesis, 0.2 mL of the Lys stock solution of typically 2 g/L was diluted 300-fold to avoid undesired aggregates during the synthesis of the biohybrids; 5 mL of the former solution was heated to 55 °C

DOI: 10.1021/jz101029f | J. Phys. Chem. Lett. 2010, 1, 2680–2687

under magnetic stirring. Then, 2.7 mL of the gold seed solution was added in order to get a [Au seed]/[protein] MR of 50. The mixture was kept at 55 °C for 2 h. Next, a number of sequential additions of suitable volumes of a solution containing $HAuCl_4$ (0.4 mM) and ascorbic acid (60 μL, 2 mM) were performed. After each addition, the mixture was left to incubate at 55 °C for 4 h. Excess reactants were eliminated by dialysis using a cellulose membrane of cutoff 100 000 Da (Spectra/Por, Netherlands).

Characterization of Metallic Hybrids. TEM images were obtained with the Phillips CM-12 transmission electron microscope operating at an accelerating voltage of 120 kV, previously described. SEM images were recorded with a LEO-435VP scanning electron microscope (Leica Microsystems GmbH, Wetlar, Germany) operating at an accelerating voltage of 30 kV. XRD experiments were carried out using a Siemens D5005 rotating anode X-ray generator. Twin Göbel mirrors were used to produce a well-collimated beam of Cu Kα radiation (λ = 1.5418 A). XRD patterns were recorded with an imaging plate detector AXS F.Nr. J2-394. Au concentrations of each biohybrid system were determined via inductively coupled plasma atomic emission spectroscopy (ICP-AES, Varian).

Catalysis of p-Nitrophenol. Typically, a reaction mixture of water (1−1.8 mL), aqueous *p*-nitrophenol solution (0.5 mL; 0.025 mM), and purified biohybrid 1 (0.2−1 mL), were first taken in a quartz cuvette. To this stirring reaction mixture, aqueous $NaBH_4$ (0.5 mL, 1 M) was then added, and the mixture was quickly placed in the cell holder of the spectrophotometer (Cary 100 Bio UV−vis, Varian Inc. Palo Alto, U.S.A.). The progress of the conversion of *p*-nitrophenol to *p*-aminophenol was then monitored via UV−vis spectroscopy by recording the time-dependent absorption spectra of the reaction mixture. The ratio of absorbance A_t of *p*-nitrophenol at time t to its value A_0 measured at t = 0 directly gives the corresponding concentration ratio (C_t/C_0) of *p*-nitrophenol. Thus, the kinetic equation of the reduction could be shown as follows

$$dC_t/dt = k_{app}t \quad \text{or} \quad \ln(C_0/C_t) = \ln(A_0/A_t) = k_{app}t$$

where C_t is the concentration of *p*-nitrophenol at time t and k_{app} is the apparent rate constant, which can be obtained from the decrease of peak intensity at 400 nm with time. Similarly, we have also carried out the reduction of *p*-nitrophenol in the presence of other biohybrids under reaction conditions similar to that used for biohybrid 1.

Recycling of the Catalyst. After the first batch of *p*-nitrophenol reduction with the metallic fibrils, the solid mass was isolated from the reaction mixture by centrifugation at 3000*g* for 15 min. The collected product was purified using two cycles of centrifugation, supernatant removal, and resuspension in water. The recovered nanohybrids were then used for further catalytic reduction of *p*-nitrophenol with $NaBH_4$, maintaining similar reaction conditions. This process was repeated five times.

SUPPORTING INFORMATION AVAILABLE Crystallyte size distributions, complementary hybrid fibrils images, and catalytic activity plots. This material is available free of charge via the Internet at http://pubs.acs.org.

AUTHOR INFORMATION

Corresponding Author:

*To whom correspondence should be addressed. E-mail: pablo.taboada@usc.es.

ACKNOWLEDGMENT Authors thank financial support from Ministerio de Ciencia e Innovación (MICINN) through Research Project MAT 2007-6107, Xunta de Galicia through Project INCITE09206020PR, and Fundación Ramón Areces through Project 2010/CL509. S.G.-L. thanks MICINN for her FPI scholarship.

REFERENCES

(1) Sepúlveda, B.; Angelomé, P. C.; Lechuga, L. M.; Liz-Marzán, L. M. LSPR-Based Nanobiosensors. *Nano Today* **2009,** *4*, 244–251.

(2) Cobley, C. M.; Skrabalak, S. E.; Xia, Y. Shape-Controlled Synthesis of Silver Nanoparticles for Plasmonic and Sensing Applications. *Plasmonics* **2009,** *4*, 171–179.

(3) Daniel, W. L.; Han, M.; Lee, J. S.; Mirkin, C. A. Colorimetric Nitrite and Nitrate Detection with Gold Nanoparticle Probes and Kinetic End Points. *J. Am. Chem. Soc.* **2009,** *131*, 6362–6363.

(4) Zheng, D.; Seferos, D. S.; Giljohann, D. A.; Patel, P. C.; Mirkin, C. A. Aptamer Nano-flares for Molecular Detection in Living Cells. *Nano Lett.* **2009,** *9*, 3258–3261.

(5) Wang, C.; Daimon, H.; Lee, Y.; Kim, J.; Sun, S. Synthesis of Monodisperse Pt Nanocubes and Their Enhanced Catalysis for Oxygen Reduction. *J. Am. Chem. Soc.* **2007,** *129*, 6974–6975.

(6) Sun, S. H.; Yang, D. Q.; Villers, D.; Zhang, G. X.; Sacher, E.; Dodelet, J. P. Template- and Surfactant-free Room Temperature Synthesis of Self-Assembled 3D Pt Nanoflowers from Single-Crystal Nanowires. *Adv. Mater.* **2008,** *20*, 571–574.

(7) Mahmoud, M. A.; Tabor, C. E.; El-Sayed, M. A.; Ding, Y.; Wang, Z. L. A New Catalytically Active Colloidal Platinum Nanocatalyst: The Multiarmed Nanostar Single Crystal. *J. Am. Chem. Soc.* **2008,** *130*, 4590–4591.

(8) Zeng, J.; Zhang, Q.; Chen, J.; Xia, Y. A Comparison Study of the Catalytic Properties of Au-Based Nanocages, Nanoboxes, and Nanoparticles. *Nano Lett.* **2010,** *10*, 30–35.

(9) Chen, J.; Wang, D.; Xi, J.; Au, L.; Siekkinen, A.; Warsen, A.; Li, Z. Y.; Zhang, H.; Xia, Y.; Li, X. Immuno Gold Nanocages with Tailored Optical Properties for Targeted Photothermal Destruction of Cancer Cells. *Nano Lett.* **2007,** *7*, 1318–1322.

(10) Cobley, C. M.; Au, L.; Chen, J.; Xia, Y. Targeting Gold Nanocages to Cancer Cells for Photothermal Destruction and Drug Delivery. *Expert Opin. Drug Delivery* **2010,** *7*, 577–587.

(11) Au, L.; Zhang, Q.; Cobley, C. M.; Gidding, M.; Schwartz, A. G.; Chen, J.; Xia, Y. Quantifying the Cellular Uptake of Antibody-Conjugated Au Nanocages by Two-Photon Microscopy and Inductively Coupled Plasma Mass Spectrometry. *ACS Nano* **2010,** *4*, 35–42.

(12) Hurst, S. J.; Han, M. S.; Lytton-Jean, A. K. R.; Mirkin, C. A. Screening the Sequence Selectivity of DNA-Binding Molecules Using a Gold Nanoparticle-Based Colorimetric Approach. *Anal. Chem.* **2007,** *79*, 7201–7205.

(13) Qian, X. M.; Nie, S. M. Single-Molecule and Single-Nanoparticle SERS: From Fundamental Mechanisms to Biomedical Applications. *Chem. Soc. Rev.* **2008,** *37*, 912–920.

(14) Zheng, G.; Daniel, W. L.; Mirkin, C. A. A New Approach to Amplified Telomerase Detection with Polyvalent Oligonucleotide Nanoparticle Conjugates. *J. Am. Chem. Soc.* **2008,** *130*, 9644–9645.

(15) Banholzer, M. J.; Millstone, J. E.; Qin, L.; Mirkin, C. A. Rationally Designed Nanostructures for Surface-Enhanced Raman Spectroscopy. *Chem. Soc. Rev.* **2008,** *37*, 885–897.
(16) Li, W.; Camargo, P. H. C.; Lu, X.; Xia, Y. Dimers of Silver Nanospheres: Facile Synthesis and Their Use as Hot Spots for Surface-Enhanced Raman Scattering. *Nano Lett.* **2009,** *9*, 485–490.
(17) Rodríguez-Lorenzo, L.; Álvarez-Puebla, R. A.; Pastoriza-Santos, I.; Mazzucco, S.; Stéphan, O.; Kociak, M.; Liz-Marzán, L. M.; García de Abajo, F. J. Zeptomol Detection Through Controlled Ultrasensitive Surface-Enhanced Raman Scattering. *J. Am. Chem. Soc.* **2009,** *131*, 4616–4618.
(18) Alvarez-Puebla, R. A.; Liz-Marzán, L. M. SERS-Based Diagnosis and Biodetection. *Small* **2010,** *6*, 604–610.
(19) van Bommel, K. J. C.; Friggeri, A.; Shinkai, S. Organic Templates for the Generation of Inorganic Materials. *Angew. Chem., Int. Ed.* **2003,** *42*, 980–999.
(20) Baron, R.; Willner, B.; Willner, I. Biomolecule−Nanoparticle Hybrids as Functional Units for Nanobiotechnology. *Chem. Commun.* **2007,** 323–332.
(21) Ofir, Y.; Samanta, B.; Rotello, V. M. Polymer and Biopolymer Mediated Self-Assembly of Gold Nanoparticles. *Chem. Soc. Rev.* **2008,** *37*, 1814–1825.
(22) Sotiropoulou, S.; Sierra-Sastre, Y.; Mark, S. S.; Batt, C. A. Biotemplated Nanostructured Materials. *Chem. Mater.* **2008,** *20*, 821–834.
(23) Behrens, S. S. Synthesis of Inorganic Nanomaterials Mediated by Protein Assemblies. *J. Mater. Chem.* **2008,** *18*, 3788–3798.
(24) Warner, M. G.; Hutchison, J. E. Linear Assemblies of Nanoparticles Electrostatically Organized on DNA Scaffolds. *Nat. Mater.* **2003,** *2*, 272–277.
(25) Gun, Q.; Chen, C.; Haynie, D. T. Cobalt Metallization of DNA: Toward Magnetic Nanowires. *Nanotechnology* **2005,** *16*, 1358–1363.
(26) Kundu, S.; Liang, H. Photochemical Synthesis of Electrically Conductive CdS Nanowires on DNA Scaffolds. *Adv. Mater.* **2008,** *20*, 826–831.
(27) Wirges, C. T.; Timper, J.; Fischler, M.; Sologubenko, A. S.; Mayer, J.; Simon, U.; Carell, T. Controlled Nucleation of DNA Metallization. *Angew. Chem., Int. Ed.* **2009,** *48*, 219–223.
(28) Knez, M.; Bittner, A. M.; Boes, F.; Wege, C.; Jeske, H.; Maiβ, E.; Kern, K. Biotemplate Synthesis of 3-nm Nickel and Cobalt Nanowires. *Nano Lett.* **2003,** *3*, 1079–1082.
(29) Dujardin, E.; Peet, C.; Stubbs, G.; Culver, J.; Mann, S. Organization of Metallic Nanoparticles Using Tobacco Mosaic Virus Templates. *Nano Lett.* **2003,** *3*, 413–417.
(30) Tsukamoto, R.; Muraoka, M.; Seki, M.; Tabata, H.; Yamashita, I. Synthesis of CoPt and $FePt_3$ Nanowires Using the Central Channel of Tobacco Mosaic Virus as a Biotemplate. *Chem. Mater.* **2007,** *19*, 2389–2391.
(31) Balci, S.; Leinberger, D. M.; Knez, M.; Bittner, A. M.; Boes, F.; Kadri, A.; Wege, C.; Jeske, H.; Kern, K. Printing and Aligning Mesoscale Patterns of *Tobacco mosaic* Virus on Surfaces. *Adv. Mater.* **2008,** *20*, 2195–2200.
(32) Fu, X.; Wang, Y.; Huang, L.; Sha, Y.; Gui, L.; Lai, L.; Tang, Y. Assemblies of Metal Nanoparticles and Self-Assembled Peptide Fibrils — Formation of Double Helical and Single-Chain Arrays of Metal Nanoparticles. *Adv. Mater.* **2003,** *15*, 902–906.
(33) Gazit, E. Self-Assembled Peptide Nanostructures: the Design of Molecular Building Blocks and Their Technological Utilization. *Chem. Soc. Rev.* **2007,** *36*, 1263–1269.
(34) Sharma, N.; Top, A.; Kiick, K. L.; Pochan, D. J. One-Dimensional Gold Nanoparticle Arrays by Electrostatically Directed Organization Using Polypeptide Self-Assembly. *Angew. Chem., Int. Ed.* **2009,** *48*, 7078–7082.
(35) Scheibel, T.; Parthasarathy, R.; Sawicki, G.; Lin, X. M.; Jaeger, H.; Lindquist, S. L. Conducting Nanowires Built by Controlled Self-Assembly of Amyloid Fibers and Selective Metal Deposition. *Proc. Natl. Acad. Sci. U.S.A.* **2003,** *100*, 4527–4532.
(36) Behrens, S.; Wu, J.; Habitch, W.; Unger, E. Silver Nanoparticle and Nanowire Formation by Microtubule Templates. *Chem. Mater.* **2004,** *16*, 3085–3090.
(37) Cherny, I.; Gazit, E. Amyloids: Not Only Pathological Agents but Also Ordered Nanomaterials. *Angew. Chem., Int. Ed.* **2008,** *47*, 4062–4069.
(38) Slocik, J. M.; Kim, S. N.; Whitehead, T. A.; Clark, D. S.; Naik, R. R. Biotemplated Metal Nanowires Using Hyperthermophilic Protein Filaments. *Small* **2009,** *5*, 2038–2042.
(39) Bigall, N. C.; Reitzing, M.; Naumann, W.; Simon, P.; van Pée, K.-H.; Eychmüller, A. Fungal Templates for Noble-Metal Nanoparticles and Their Application in Catalysis. *Angew. Chem., Int. Ed.* **2008,** *47*, 7876–7879.
(40) Retches, M.; Gazit, E. Casting Metal Nanowires Within Discrete Self-Assembled Peptide Nanotubes. *Science* **2003,** *300*, 625–627.
(41) Kinsella, J. M.; Ivanisevic, A. Enzymatic Clipping of DNA Wires Coated with Magnetic Nanoparticles. *J. Am. Chem. Soc.* **2005,** *127*, 3276–3277.
(42) Bai, H.; Xu, K.; Xu, Y.; Matsui, H. Fabrication of Au Nanowires of Uniform Length and Diameter Using a Monodisperse and Rigid Biomolecular Template: Collagen-like Triple Helix. *Angew. Chem., Int. Ed.* **2007,** *46*, 3319–3322.
(43) Ostrov, N.; Gazit, E. Genetic Engineering of Biomolecular Scaffolds for the Fabrication of Organic and Metallic Nanowires. *Angew. Chem., Int. Ed.* **2010,** *49*, 3018–3021.
(44) Guha, S.; Banerjee, A. Self-Assembled Robust Dipeptide Nanotubes and Fabrication of Dipeptide-Capped Gold Nanoparticles on the Surface of these Nanotubes. *Adv. Funct. Mater.* **2009,** *19*, 1949–1961.
(45) Ryu, J.; Lim, S. Y.; Park, C. B. Photoluminescent Peptide Nanotubes. *Adv. Mater.* **2009,** *11*, 1577–1581.
(46) Górzny, M. L.; Walton, A. S.; Evans, S. D. Synthesis of High-Surface-Area Platinum Nanotubes Using a Viral Template. *Adv. Funct. Mater.* **2010,** *20*, 1295–1300.
(47) Balci, S.; Noda, K.; Bittner, A.; Kadri, A.; Wege, C.; Jeske, H.; Kern, K. Self-Assembly of Metal-Virus Nanodumbbells. *Angew. Chem., Int. Ed.* **2007,** *46*, 3149–3151.
(48) Dobson, C. M. Protein Folding and Misfolding. *Nature* **2003,** *426*, 884–890.
(49) Jahn, T. R.; Radford, S. E. Folding Versus Aggregation: Polypeptide Conformations on Competing Pathways. *Arch. Biochem. Biophys.* **2008,** *469*, 100–117.
(50) Frare, E.; De Laureto, P. P.; Zurdo, J.; Dobson, C. M.; Fontana, A. A Highly Amyloidogenic Region of Hen Lysozyme. *J. Mol. Biol.* **2004,** *340*, 1153–1165.
(51) Pawar, A. P.; Dubai, K. F.; Zurdo, J.; Chiti, F.; Vendruscolo, M.; Dobson, C. M. Prediction of "Aggregation-Prone" and "Aggregation-Susceptible" Regions in Proteins Associated with Neurodegenerative Diseases. *J. Mol. Biol.* **2005,** *350*, 379–392.
(52) Lieu, V. H.; Wu, J. W.; Wang, S. S. S.; Wu, C. H. Inhibition of Amyloid Fibrillization of Hen Egg-White Lysozymes by Rifampicin and *p*-Benzoquinone. *Biotechnol. Prog.* **2007,** *23*, 698–706.
(53) Yu, L.; Banerjee, I. A.; Shima, A.; Rajan, K.; Matsui, H. Size-Controlled Ni Nanocrystal Growth on Peptide Nanotubes and Their Magnetic Properties. *Adv. Mater.* **2004,** *16*, 709–712.

DOI: 10.1021/jz101029f | *J. Phys. Chem. Lett.* **2010,** *1*, 2680–2687

(54) Almeida, N. L.; Oliveira, C. L. P.; Torriani, I. L.; Loh, W. Calorimetric and Structural Investigation of the Interaction of Lysozyme and Bovine Serum Albumin with Poly(Ethylene Oxide) and its Copolymers. *Colloids Surf., B* **2004,** *38*, 67–76.
(55) Dutta, P.; Manivannan, A.; Seehra, M. S.; Shah, N.; Huffman, G. P. Magnetic Properties of Nearly Defect-Free Maghemite Nanocrystals. *Phys. Rev. B* **2004,** *70*, 174428/1–174428/7.
(56) Shiomi, T.; Tsunoda, T.; Kawai, A.; Mizukami, F.; Sakaguchi, K. Biomimetic Synthesis of Lysozyme−Silica Hybrid Hollow Particles Using Sonochemical Treatment: Influence of pH and Lysozyme Concentration on Morphology. *Chem. Mater.* **2007,** *19*, 4486–4493.
(57) Schrinner, M.; Ballauff, M.; Talmon, Y.; Kauffmann, Y.; Thun, J.; Moller, M.; Breu, J. Dynamical Quorum Sensing and Synchronization in Large Populations of Chemical Oscillators. *Science* **2009,** *323*, 617–620.
(58) Qin, G.; W. Pei, W.; Ma, X.; Xu, X.; Ren, Y.; Sun, W.; Zuo, L. Enhanced Catalytic Activity of Pt Nanomaterials: From Monodisperse Nanoparticles to Self-Organized Nanoparticle-Linked Nanowires. *J. Phys. Chem. C* **2010,** *114*, 6909–6913.
(59) Hayakawa, K.; Yoshimura, T.; Esumi, K. Preparation of Gold-Dendrimer Nanocomposites by Laser Irradiation and Their Catalytic Reduction of 4-Nitrophenol, Immobilization and Recovery of Au Nanoparticles from Anion Exchange Resin: Resin-Bound Nanoparticle Matrix as a Catalyst for the Reduction of 4-Nitrophenol. *Langmuir* **2003,** *19*, 5517–5521.
(60) Praharaj, S.; Nath, S.; Gosh, S. K.; Kundu, S.; Pal, T. Immobilization and Recovery of Au Nanoparticles from Anion Exchange Resin: Resin-Bound Nanoparticle Matrix as a Catalyst for the Reduction of 4-Nitrophenol. *Langmuir* **2004,** *20*, 9889–9892.
(61) Rashid, M. H.; Bhattacharjee, R. R.; Kotal, A.; Mandal, T. K. Synthesis of Spongy Gold Nanocrystals with Pronounced Catalytic Activities. *Langmuir* **2006,** *22*, 7141–7143.
(62) Rashid, M. H.; Mandal, T. K. Organic Ligand-Mediated Synthesis of Shape-Tunable Gold Nanoparticles: An Application of Their Thin Film as Refractive Index Sensors. *J. Phys. Chem. C* **2007,** *111*, 9684–9693.
(63) Esumi, K.; Isono, R.; Yoshimura, T. Preparation of PAMAM− and PPI−Metal (Silver, Platinum, and Palladium) Nanocomposites and Their Catalytic Activities for Reduction of 4-Nitrophenol. *Langmuir* **2004,** *20*, 237–243.
(64) Liu, J.; Qin, G.; Raavendran, P.; Ikushima, Y. Facile "Green" Synthesis, Characterization, and Catalytic Function of β-D-Glucose-Stabilized Au Nanocrystals. *Chem.—Eur. J.* **2006,** *12*, 2131–2138.
(65) Chen, X.; Zhao, D.; An, Y.; Shi, L.; Hou, W.; Chen, L. Catalytic Properties of Gold Nanoparticles Immobilized on the Surfaces of Nanocarriers. *J. Nanopart. Res.* **2010,** *12*, 1877–1887.
(66) Li, L.; Wang, Z.; Huang, T.; Xie, J.; Qin, L. Porous Gold Nanobelts Templated by Metal−Surfactant Complex Nanobelts. *Langmuir* **2010,** *26*, 12330–12335.
(67) Bai, X.; Gao, Y.; Liu, H.-g.; Zheng, L. Synthesis of Amphiphilic Ionic Liquids Terminated Gold Nanorods and Their Superior Catalytic Activity for the Reduction of Nitro Compounds. *J. Phys. Chem. C* **2009,** *113*, 17730–17736.
(68) Wang, Y.; Wei, G.; Zhang, W.; Jiang, X.; Zheng, P.; Shi, L.; Dong, A. Responsive Catalysis of Thermoresponsive Micelle-Supported Gold Nanoparticles. *J. Mol. Catal. A: Chem.* **2007,** *266*, 233–238.
(69) Chen, X.; An, Y.; Zhao, D.; He, Z.; Zhang, Y.; Cheng, J.; Shi, L. Core−Shell−Corona Au−Micelle Composites with a Tunable Smart Hybrid Shell. *Langmuir* **2008,** *24*, 8198–8204.
(70) Hain, J.; Schrinner, M.; Lu, Y.; Pich, A. Design of Multicomponent Microgels by Selective Deposition of Nanomaterials. *Small* **2008,** *4*, 2016–2024.
(71) Huang, T.; Meng, F.; Qi, L. Facile Synthesis and One-Dimensional Assembly of Cyclodextrin-Capped Gold Nanoparticles and Their Applications in Catalysis and Surface-Enhanced Raman Scattering. *J. Phys. Chem. C* **2009,** *113*, 13636–13642.
(72) Lee, J.; Park, L. C.; Song, H. A Nanoreactor Framework of a Au@SiO_2 Yolk/Shell Structure for Catalytic Reduction of *p*-Nitrophenol. *Adv. Mater.* **2008,** *20*, 1523–1528.
(73) Rashid, M. H.; Mandal, T. K. Templateless Synthesis of Polygonal Gold Nanoparticles: An Unsupported and Reusable Catalyst with Superior Activity. *Adv. Funct. Mater.* **2008,** *18*, 2261–2271.
(74) Kumar, S. S.; Kumar, C. S.; Mathiyarasu, J.; Phani, K. L. Stabilized Gold Nanoparticles by Reduction Using 3,4-Ethylenedioxythiophene-polystyrenesulfonate in Aqueous Solutions: Nanocomposite Formation, Stability, and Application in Catalysis. *Langmuir* **2007,** *23*, 3401–3408.
(75) Burda, C.; Chen, X.; Narayanan, R.; El-Sayed, M. A. Chemistry and Properties of Nanocrystals of Different Shapes. *Chem. Rev.* **2005,** *105*, 1025–1102.
(76) Knubovets, T.; Osterhout, J. J.; Connolly, P. J.; Klibanov, A. M. Structure, Thermostability, And Conformational Flexibility of Hen Egg-White Lysozyme Dissolved in Glycerol. *Proc. Natl. Acad. Sci. U.S.A.* **1999,** *96*, 1262–1267.

DOI: 10.1021/jz101029f | *J. Phys. Chem. Lett.* **2010,** *1*, 2680–2687